Ultrafast Raman thermometry in driven $YBa_2Cu_3O_{6.48}$

T.-H. Chou,[1] M. Först,[1] M. Fechner,[1] M. Henstridge,[1,2] S. Roy,[1] M. Buzzi,[1] D. Nicoletti,[1] Y. Liu,[3] S. Nakata,[3] B. Keimer,[3] and A. Cavalleri[1,4,*]

[1]*Max Planck Institute for the Structure and Dynamics of Matter, 22761 Hamburg, Germany*
[2]*SLAC National Accelerator Laboratory, Menlo Park, California 94025, USA*
[3]*Max Planck Institute for Solid State Research, 70569 Stuttgart, Germany*
[4]*Department of Physics, Clarendon Laboratory, University of Oxford, Oxford OX1 3PU, United Kingdom*

(Received 29 September 2023; revised 18 April 2024; accepted 22 April 2024; published 13 May 2024)

Signatures of photoinduced superconductivity have been reported in cuprate materials subjected to a coherent phonon drive. A "cold" superfluid was extracted from the transient Terahertz conductivity and was seen to coexist with "hot" uncondensed quasiparticles, a hallmark of a driven-dissipative system of which the interplay between coherent and incoherent responses is not well understood. Here, time resolved spontaneous Raman scattering was used to probe the lattice temperature in the photoinduced superconducting state of $YBa_2Cu_3O_{6.48}$. An increase in lattice temperature of up to 140 K was observed by measuring the time dependent Raman scattering intensity of an undriven "spectator" phonon mode. This value is consistent with the estimated increase in quasiparticle temperature measured under the same excitation conditions. These temperature changes provide quantitative information on the nature of the driven state and its decay, and may suggest a strategy to optimize this effect.

DOI: 10.1103/PhysRevB.109.195141

I. INTRODUCTION

The equilibrium superconducting transition in cuprate superconductors is characterized by a number of features in the terahertz-frequency optical response [1–4]. For normal state $YBa_2Cu_3O_{6+x}$ ($T > T_c$), the real part of the optical conductivity $\sigma_1(\omega)$ exhibits a featureless spectrum with a finite value, which descends from the Drude response of quasiparticles at frequencies below the scattering rate ($\omega \ll 1/\tau$). Along the c axis of $YBa_2Cu_3O_{6+x}$, where one finds a semiconducting normal state response, this feature reflects the population of thermally excited quasiparticles [5,6]. Upon cooling into the superconducting state, the $\sigma_1(\omega)$ spectral weight in the frequency range below the superconducting energy gap is reduced, and a divergent $1/\omega$ response in the imaginary part of the optical conductivity $\sigma_2(\omega)$ appears, indicating the onset of dissipationless transport.

When midinfrared pulses are used to resonantly drive apical oxygen phonons in the normal state ($T > T_c$) of underdoped $YBa_2Cu_3O_{6+x}$, changes in the terahertz optical properties are observed with the same $1/\omega$ divergence in the transient $\sigma_2(\omega)$, connected to nonequilibrium superconductinglike properties [7–10]. Figures 1(a) and 1(b) display one example of these induced optical conductivity features, measured along the c axis of $YBa_2Cu_3O_{6.48}$ at $T = 100$ K, showing the equilibrium state (gray line) and the light-induced state (colored circles) [11]. The latter was calculated using two different models, one based on a linear dependence of the photoinduced response on the pump fluence (blue) and a second one based on a square root dependence (light green), obtaining responses of different magnitudes but identical in quality [12,13].

The nature of this nonequilibrium state was recently studied in a series of complementary experiments, based on time-resolved measurements of the near-infrared reflectivity $R(t)$ and the second-order nonlinear optical susceptibility $\chi^{(2)}(t)$. These studies revealed a number of coherently oscillating normal modes, including three coherent Raman-active phonons at frequencies of 3.7, 4.6, and 5.1 THz [Fig. 1(d), gray [14–16]], two resonantly driven infrared-active phonons at 17.5 and 20 THz [Fig. 1(d), orange], and, most importantly, two electronic modes at 2.5 and 14 THz [Fig. 1(d), red]. The two coherent electronic modes were assigned to amplified interbilayer and intrabilayer Josephson plasmons [16]. The diagram in Fig. 1(e) summarizes the current understanding of these coherent couplings [16,17].

II. EXPERIMENT AND RESULTS

The present study focuses on *incoherent* energy transfer in driven $YBa_2Cu_3O_{6.48}$. Firsty, the midinfrared excitation pulses not only drive coherent phonons but also excite charge carriers, which in turn couple to other modes of the system, including phonons, spin excitations, and plasma modes. Figure 2(a) depicts schematically the expected quasiparticle heating, represented by the corresponding electron density of states (eDOS) and population $n(E)$. Second, one expects

*andrea.cavalleri@mpsd.mpg.de

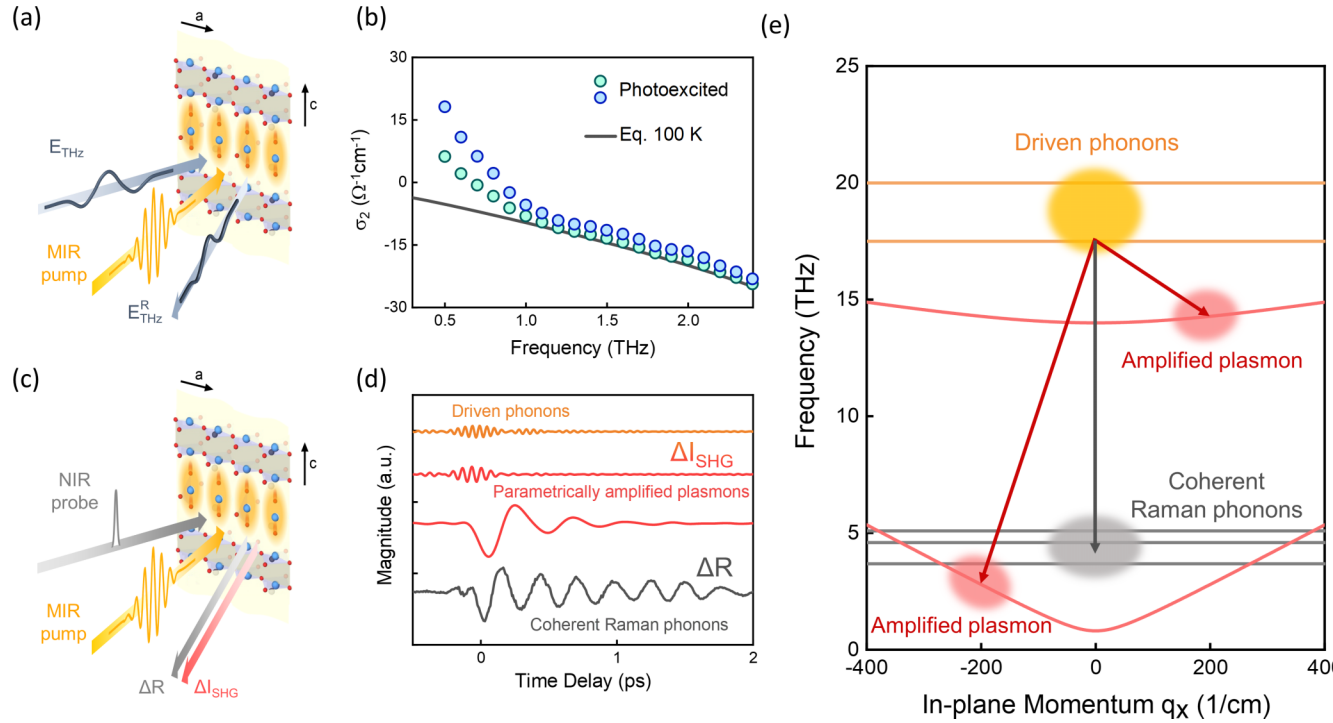

FIG. 1. Coherent couplings in optically driven $YBa_2Cu_3O_{6.48}$. (a) Schematic of time-resolved terahertz spectroscopy. The midinfrared pump pulse (yellow) resonantly drives infrared-active c-axis apical oxygen phonons in $YBa_2Cu_3O_{6.48}$. Single-cycle terahertz probe pulses (slate gray) were reflected from the sample and detected by phase-sensitive electro-optic sampling. (b) Imaginary part of the c-axis optical conductivity $\sigma_2(\omega)$, measured in $YBa_2Cu_3O_{6.48}$ at $T = 100$ K. Gray line and colored circles show the equilibrium and transient $\sigma_2(\omega)$, respectively. The latter was calculated from the data in Ref. [11] with two different models, one based on a linear (blue) and one based on a square root (light green) dependence of the photoinduced response on the pump fluence [12,13]. (c) Schematic of time-resolved optical spectroscopy. The pump pulse (yellow) is the same as in (a). Near-infrared probe pulses (gray) were detected in reflection geometry. Gray and red arrows represent reflectivity changes at the fundamental frequency (ΔR) and intensity changes of second harmonic generation ΔI_{SHG}, respectively. (d) ΔR (gray) shows an oscillatory response at the Raman phonon frequencies. These data were reproduced from Ref. [16] Fig. 1(b) after subtraction of a slowly varying background. ΔI_{SHG} shows instead coherent oscillations of the driven infrared-active phonons (orange) and parametrically amplified intrabilayer and interbilayer Josephson plasma polaritons (red). These data were reproduced from Ref. [16] Fig. 2(e), having applied Fourier transform band pass filters with frequency windows of 0-5, 12-17, and 17-22 THz. (e) Frequency-momentum diagram showing the dispersion curves of driven infrared phonons (orange), Josephson plasmons (light red), and Raman phonons (light gray). The dark gray arrow shows the coupling pathway of stimulated ionic Raman processes between the driven phonons and Raman phonons. The dark red arrows indicate instead the three-mode mixing process between driven phonons and Josephson plasmons.

that the coherently driven phonons will also decay into incoherent vibrational modes through spontaneous ionic Raman processes, which will raise the temperature of many low-energy degrees of freedom. As an example of these dissipative dynamics, we focus here on a high-frequency Raman mode at 15 THz [18,19], whose period is too high to be excited coherently by the midinfrared pump pulses [14,20].

To estimate the incoherent response of hot quasiparticles, we tracked the $\sigma_1(\omega)$ conductivity spectra at different time delays after the optical excitation. Following the same analysis as reported in Ref. [11], we calculated the $\sigma_1(\omega)$ spectral weight between 0.6 and 2.25 THz (20–75 cm^{-1}) as $\int_{0.6\ \mathrm{THz}}^{2.25\ \mathrm{THz}} \sigma_1(\omega) d\omega$ to determine the normal fluid density. Then, we compared the value of this integral to its equilibrium values taken at different temperatures to infer an "equivalent temperature" of the quasiparticles. The time evolution of these transient spectral weights [Fig. 2(c)] shows that the quasiparticles undergo a temperature increase ΔT between 100 K and 200 K, depending on the model used to extract the optical properties, and decay back to the equilibrium temperature in about 5 ps. Although this estimate is by no means a precise measurement of the quasiparticle temperature, it provides a useful point of reference.

Here, we complement the measurements reported above with time-resolved spontaneous Raman scattering experiments [21–30] to probe the lattice temperature under the same midinfrared excitation condition. For these experiments, we focused on measurements of a "spectator mode," not excited directly by the pump and with frequencies that were high enough to prevent their coherent excitation (only possible for phonon modes with full periods longer than twice the pump pulse duration).

Figure 3(a) shows a schematic of our time-resolved Raman scattering setup. The $YBa_2Cu_3O_{6.48}$ crystal was excited by 800-fs midinfrared pulses, centered at 20 THz frequency and polarized along the crystal c axis to resonantly drive the infrared-active apical oxygen phonons that induce the transient superconducting state. Probe pulses with 405-nm wavelength, 600-fs time duration, and 100-cm^{-1} bandwidth were used for the Raman scattering process. The probe

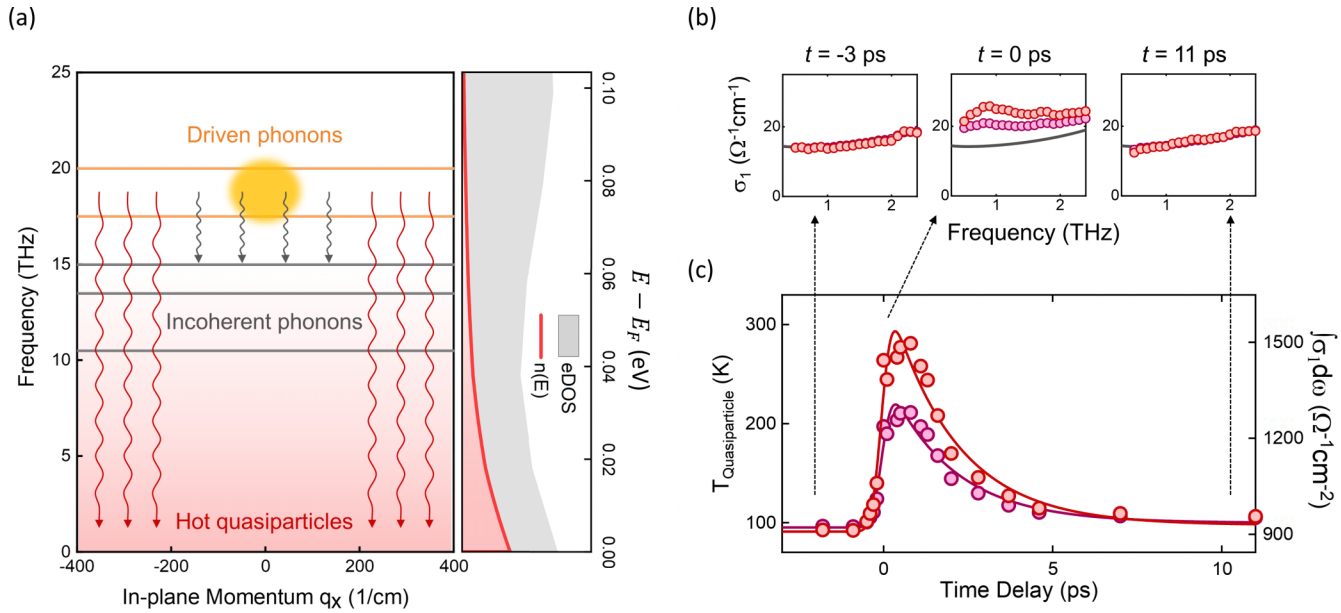

FIG. 2. Incoherent couplings in optically driven $YBa_2Cu_3O_{6.48}$. (a) Left panel: Frequency-momentum diagram with the dispersion curves of resonantly driven infrared phonons (orange), and incoherent Raman phonons at 10.5, 13.5, and 15 THz [18,19] (light gray). The red gradient background represents the electron distribution above the Fermi energy, which is at zero frequency in this diagram. The wiggling arrows indicate the incoherent energy transfer to Raman phonons (dark gray) and quasiparticles (dark red). Right panel: Electron density of states eDOS (gray) and population $n(E)$ (red). The former was obtained by *ab initio* calculations, while the latter was calculated by multiplying the eDOS with a Fermi-Dirac distribution at $T = 100$ K. (b) Real part of the c-axis optical conductivity, $\sigma_1(\omega)$, of $YBa_2Cu_3O_{6.48}$ measured at time delays of $t = -3$, 0, and $+11$ ps. In each panel, gray line and colored circles represent the equilibrium and transient $\sigma_1(\omega)$ at $T = 100$ K, respectively. The latter was calculated from the data of Ref. [11] with two different models, one based on a linear dependence (red) and another one based on a square root dependence (purple) of the photoinduced response on the pump fluence [12,13]. (c) Equivalent quasiparticle temperature as a function of time delay (colored circles), determined from the integrated spectral weight $\int_{0.6\ \mathrm{THz}}^{2.25\ \mathrm{THz}} \sigma_1(\omega)d\omega$ (see right axis). Red and purple circles refer to the two models introduced in (b) with the same color coding. Full lines are fits with an error function and an exponential decay.

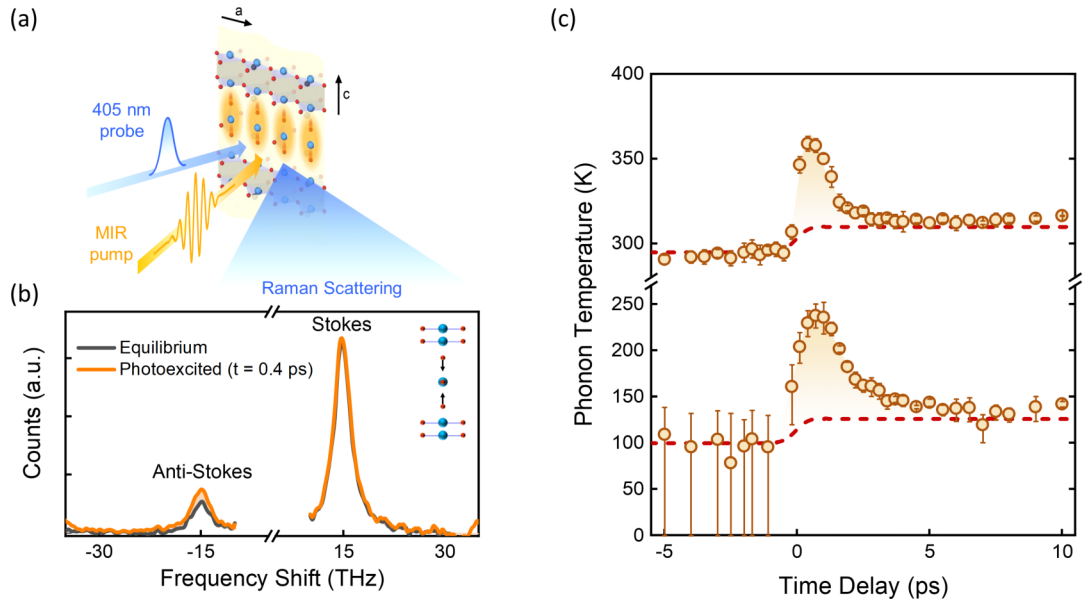

FIG. 3. (a) Schematic of time-resolved spontaneous Raman spectroscopy. The pump (yellow) is the same as in Fig. 1. 405-nm probe pulses (blue) were used for the Raman scattering process. The scattered photons were spectrally analyzed. (b) The Raman spectra were measured at $T = 295$ K at equilibrium (black) and after photoexcitation (orange). The displayed data were obtained by subtracting background spectra and high-order side peaks from the raw data (see Supplemental Material S2 [32]). The peaks at ± 15 THz represent the Stokes (+) and Anti-Stokes (−) responses of the A_g symmetry apical oxygen Raman mode. Inset: atomic motions along the c-axis apical oxygen Raman-active mode coordinates. (c) Zero-fluence phonon temperatures as a function of time delay. These data were measured at cryostat base temperatures of 295 K (upper) and 100 K (lower). The dashed red lines were obtained from heating calculation (see Supplemental Material S5 [32]).

photons, scattered from the sample, were analyzed by a spectrometer equipped with a thermoelectric-cooled charge-coupled device camera. All Raman spectra presented in this paper were acquired in the backscattering geometry, with both the input probe pulses and the scattered photons polarized along the $YBa_2Cu_3O_{6.48}$ c axis.

Figure 3(b) displays the Raman spectrum obtained at equilibrium condition (gray line). We find the Stokes (S) and anti-Stokes (AS) peaks of the apical oxygen A_{1g} phonon at ± 15 THz, which are offset in frequency from the coherently driven infrared-active B_{1u} symmetry mode around 20 THz. The pumped Raman spectrum taken at time delay $t = 0.4$ ps (orange line) shows an enhancement in the amplitude of the AS peak, while the S peak barely changed, indicating an increase of the phonon temperature after the midinfrared excitation.

The intensity ratio of the AS and S peaks, I_{AS}/I_S, is related to the distribution of phonon populations in the ground state and the first excited state and allows us to calculate the temperature of this Raman mode using [31]

$$\frac{I_{AS}}{I_S} = \frac{(\omega_0 + \omega_{ph})^3}{(\omega_0 - \omega_{ph})^3}\frac{n}{n+1} = \frac{(\omega_0 + \omega_{ph})^3}{(\omega_0 - \omega_{ph})^3} e^{-\hbar\omega_{ph}/k_B T_{ph}}. \quad (1)$$

Here, ω_0 is the central frequency of the probe pulses, ω_{ph} is the frequency of the Raman mode, k_B is the Boltzmann constant, and T_{ph} is the phonon temperature defined by the occupation number $n = (e^{\hbar\omega_{ph}/k_B T_{ph}} - 1)^{-1}$ based on the Bose-Einstein distribution. The cubic term in Eq. (1) arises from the frequency dependence of the Raman scattering cross section $\sigma_R \propto \omega^4$. Note that the photon counting detector used here, for which the read-out signal strength is proportional to the total photon number rather than the total energy, requires us to use a cubic instead of a quartic term [31].

In our experiments at a laser repetition rate of 1 kHz, the probe fluences were set between 0.8 and 2 mJ/cm^2 to ensure sufficient numbers of scattered photons for data acquisition. However, such high probe fluences unavoidably introduce additional sample heating and potentially induce other nonlinear effects. For an accurate measurement of the phonon temperatures, it is therefore crucial to characterize the effect of the probe pulses on the time-dependent Raman spectra. We conducted midinfrared pump Raman probe experiments using multiple probe fluences. By linearly fitting the fluence-dependent AS/S intensity ratios, we extrapolated the "zero-fluence" phonon temperature for each time delay. This approach minimized the influence of the probe-induced heating and revealed the accurate phonon temperatures. The details of data processing and analysis are shown in Supplemental Material S2 and S3 [32].

Figure 3(c) shows the time evolutions of the zero-fluence phonon temperatures in $YBa_2Cu_3O_{6.48}$ measured at base temperatures of 295 and 100 K. Both transients display a prompt rise in phonon temperature near time zero followed by an exponential decay to a finite temperature, which can be interpreted as the thermalization of this phonon with other degrees of freedom in the system. We first focus on the data at long positive time delays (>5 ps). Here, we expect the different degrees of freedom in the material to have reached thermalization, and we compare the measured temperature change to a

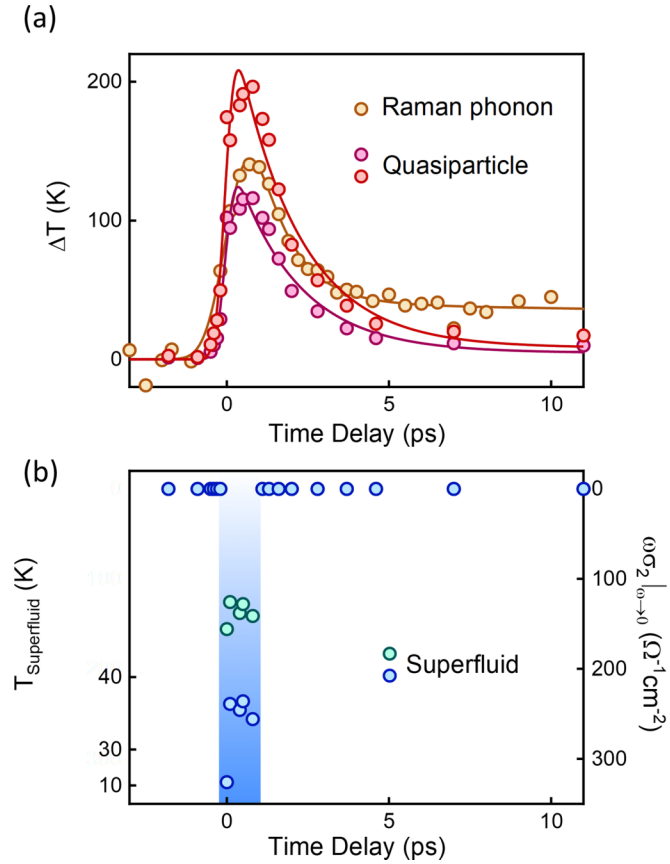

FIG. 4. (a) Temperature changes of quasiparticles and Raman phonons as a function of time delay. The solid lines are fits to the data with a model including an error function and an exponential decay. The red and purple circles refer to different models used to extract the terahertz (quasiparticle) response, assuming a linear or a square-root dependence as a function of pump fluence, respectively [12,13]. (b) Equivalent temperatures of the superfluid as a function of time delay [11]. The blue shaded area highlights the time delay window within which a transient superconductinglike response was observed. The equivalent temperature of the superfluid was determined from $\lim_{\omega\to 0} \omega\sigma_2(\omega)$ (values reported on the right axis), using the same models discussed in (a) to calculate the terahertz response, i.e., linear (blue circles) or square-root (light green circles).

calculation based on the total energy absorbed by the sample, the excited volume, and the heat capacity (see Supplemental Material S5 for details [32]). For a midinfrared excitation density of 8 mJ/cm^2, shown as the red dashed line in Fig. 3(c), the calculated temperature of the $YBa_2Cu_3O_{6.48}$ surface increased from 295 K (100 K) and thermalized at 310 K (125 K). The measured phonon temperatures at negative and long positive time delay agree with the calculation.

We next turn to the results at earlier time delays, that is before thermalization. A nonequilibrium phonon temperature of 360 K was measured at the peak of the signal for the base temperature of 295 K, well above the equilibrated temperature of 310 K at longer delays. In the case of 100 K base temperature, an initial overshoot up to 240 K was observed, followed by thermal equilibration to 125 K on the longer time scale. These peak temperatures are far lower than what reported for near-infrared excitation in Ref. [28] at similar

excitation fluences. At 100 K base temperature, the transient lattice temperature increase of 140 K broadly compatible with the quasiparticle temperature overshoot extracted from the measurements of the optical conductivity $\sigma_1(\omega, t)$, and both show similar decay time constants of ∼1.3 ps.

Given that our time-resolved Raman experiment might underestimate the peak lattice temperature due to the 600-fs probe pulse, we conducted a deconvolution analysis on the Raman data [Fig. 3(c)] to achieve a more precise estimation (see Supplemental Material S4 [32]). The results indicate that the maximum increase in lattice temperature for the driven $YBa_2Cu_3O_{6.48}$ at 100 K is approximately 150 K.

These incoherent "hot" degrees of freedom are to be compared to the dynamics of the superfluid, manifested in the strength of the divergent imaginary part of the optical conductivity $\sigma_2(\omega)$. In Ref. [11], the time delay dependent $\sigma_2(\omega)$ spectra were used to calculate values of $\lim_{\omega\to 0}\omega\sigma_2(\omega)$, which is directly related to the superfluid density. By comparing these values with equilibrium optical conductivity spectra taken at multiple temperatures below T_c, the "equivalent temperature" of the superfluid was extracted in that work. The time evolution of the coherent superfluid in response to the midinfrared excitation is presented in Fig. 4(b). In contrast to the longer-lived effects observed on incoherent phonons and quasiparticles, the equivalent "cooling" of superfluid only persists within the duration of pump pulse.

III. DISCUSSION

Figure 4(a) depicts the temperature changes of quasiparticles and phonons. Within the uncertainty introduced by the choice of model to extract $T_{\text{Quasiparticle}}$ from the data in Ref. [11], the values are largely compatible throughout the whole dynamics. At least two scenarios emerge at this stage. A stronger superfluid *vis-à-vis* hot carriers and hot lattice may connect the present physics to the well-known microwave enhanced superconductivity mechanism [35]. However, this appears unlikely in the present context as the effect is far too large to be explained by the Eliashberg mechanism [36] and the observed response is resonant with the optical phonon drive. A second scenario, which we believe is more likely, would be one in which both the hot quasiparticles and the hot phonons are detrimental to the coherent state, whichever mechanism one may invoke. In this picture, quasiparticles and phonons have comparable influences on the decoherence time of the light induced superconductinglike state. As the lifetime of the coherent phase is never observed to be longer than the optical pulse [11], one should focus on optimizing the conditions of the drive to minimize the excitation of hot carriers. Suitably shaped pump pulses or trains of pump pulses may provide a stronger and longer-lived photoinduced state.

ACKNOWLEDGMENTS

We acknowledge support from the Deutsche Forschungsgemeinschaft (DFG; German Research Foundation) via the excellence cluster "CUI: Advanced Imaging of Matter" (EXC 2056, Project No. 390715994) and the priority program SFB925 (Project No. 170620586).

[1] D. N. Basov and T. Timusk, Electrodynamics of high-T_c superconductors, Rev. Mod. Phys. **77**, 721 (2005).

[2] C. C. Homes, T. Timusk, D. A. Bonn, R. Liang, and W. N. Hardy, Optical phonons polarized along the c axis of $YBa_2Cu_3O_{6+x}$, for $x = 0.5 \to 0.95$, Can. J. Phys. **73**, 663 (1995).

[3] C. C. Homes, T. Timusk, D. A. Bonn, R. Liang, and W. N. Hardy, Optical properties along the c-axis of $YBa_2Cu_3O_{6+x}$, for x = 0.50 → 0.95 evolution of the pseudogap, Phys. C (Amsterdam, Neth.) **254**, 265 (1995).

[4] D. N. Basov, S. I. Woods, A. S. Katz, E. J. Singley, R. C. Dynes, M. Xu, D. G. Hinks, C. C. Homes, and M. Strongin, Sum rules and interlayer conductivity of high-T_c cuprates, Science **283**, 49 (1999).

[5] M. C. Nuss, P. M. Mankiewich, M. L. O'Malley, E. H. Westerwick, and P. B. Littlewood, Dynamic conductivity and coherence peak in $YBa_2Cu_3O_7$ superconductors, Phys. Rev. Lett. **66**, 3305 (1991).

[6] A. Pimenov, A. Loidl, G. Jakob, and H. Adrian, Optical conductivity in $YBa_2Cu_3O_{7-\delta}$ thin films, Phys. Rev. B **59**, 4390 (1999).

[7] S. Kaiser, C. R. Hunt, D. Nicoletti, W. Hu, I. Gierz, H. Y. Liu, M. Le Tacon, T. Loew, D. Haug, B. Keimer, and A. Cavalleri, Optically induced coherent transport far above T_c in underdoped $YBa_2Cu_3O_{6+\delta}$, Phys. Rev. B **89**, 184516 (2014).

[8] W. Hu, S. Kaiser, D. Nicoletti, C. R. Hunt, I. Gierz, M. C. Hoffmann, M. Le Tacon, T. Loew, B. Keimer, and A. Cavalleri, Optically enhanced coherent transport in $YBa_2Cu_3O_{6.5}$ by ultrafast redistribution of interlayer coupling, Nat. Mater. **13**, 705 (2014).

[9] C. R. Hunt, D. Nicoletti, S. Kaiser, D. Pröpper, T. Loew, J. Porras, B. Keimer, and A. Cavalleri, Dynamical decoherence of the light induced interlayer coupling in $YBa_2Cu_3O_{6+\delta}$, Phys. Rev. B **94**, 224303 (2016).

[10] B. Liu, M. Först, M. Fechner, D. Nicoletti, J. Porras, T. Loew, B. Keimer, and A. Cavalleri, Pump frequency resonances for light-induced incipient superconductivity in $YBa_2Cu_3O_{6.5}$, Phys. Rev. X **10**, 011053 (2020).

[11] A. Ribak, M. Buzzi, D. Nicoletti, R. Singla, Y. Liu, S. Nakata, B. Keimer, and A. Cavalleri, Two-fluid dynamics in driven $YBa_2Cu_3O_{6.48}$, Phys. Rev. B **107**, 104508 (2023).

[12] J. S. Dodge, L. Lopez, and D. G. Sahota, Optical saturation produces spurious evidence for photoinduced superconductivity in K_3C_{60}, Phys. Rev. Lett. **130**, 146002 (2023).

[13] M. Buzzi, D. Nicoletti, E. Rowe, E. Wang, and A. Cavalleri, Comment on arXiv:2210.01114: Optical saturation produces spurious evidence for photoinduced superconductivity in K_3C_{60}, arXiv:2303.10169.

[14] R. Mankowsky, M. Först, T. Loew, J. Porras, B. Keimer, and A. Cavalleri, Coherent modulation of the $YBa_2Cu_3O_{6+x}$ atomic

structure by displacive stimulated ionic Raman scattering, Phys. Rev. B **91**, 094308 (2015).

[15] R. Mankowsky, A. Subedi, M. Först, S. O. Mariager, M. Chollet, H. T. Lemke, J. S. Robinson, J. M. Glownia, M. P. Minitti, A. Frano, M. Fechner, N. A. Spaldin, T. Loew, B. Keimer, A. Georges, and A. Cavalleri, Nonlinear lattice dynamics as a basis for enhanced superconductivity in $YBa_2Cu_3O_{6.5}$, Nature (London) **516**, 71 (2014).

[16] A. von Hoegen, M. Fechner, M. Först, N. Taherian, E. Rowe, A. Ribak, J. Porras, B. Keimer, M. Michael, E. Demler, and A. Cavalleri, Amplification of superconducting fluctuations in driven $YBa_2Cu_3O_{6+x}$, Phys. Rev. X **12**, 031008 (2022).

[17] M. H. Michael, A. von Hoegen, M. Fechner, M. Först, A. Cavalleri, and E. Demler, Parametric resonance of Josephson plasma waves: A theory for optically amplified interlayer superconductivity in $YBa_2Cu_3O_{6+x}$, Phys. Rev. B **102**, 174505 (2020).

[18] M. N. Iliev, V. G. Hadjiev, S. Jandl, D. Le Boeuf, V. N. Popov, D. Bonn, R. Liang, and W. N. Hardy, Raman study of twin-free ortho-II $YBa_2Cu_3O_{6.5}$ single crystals, Phys. Rev. B **77**, 174302 (2008).

[19] S. Hong, H. Cheong, and G. Park, Raman analysis of a $YBa_2Cu_3O_{7-\delta}$ thin film with oxygen depletion, Phys. C (Amsterdam, Neth.) **470**, 383 (2010).

[20] M. Först, C. Manzoni, S. Kaiser, Y. Tomioka, Y. Tokura, R. Merlin, and A. Cavalleri, Nonlinear phononics as an ultrafast route to lattice control, Nat. Phys. **7**, 854 (2011).

[21] D. von der Linde, J. Kuhl, and H. Klingenberg, Raman scattering from nonequilibrium LO phonons with picosecond resolution, Phys. Rev. Lett. **44**, 1505 (1980).

[22] J. A. Kash, J. C. Tsang, and J. M. Hvam, Subpicosecond time-resolved Raman spectroscopy of LO phonons in GaAs, Phys. Rev. Lett. **54**, 2151 (1985).

[23] D. Song, F. Wang, G. Dukovic, M. Zheng, E. D. Semke, L. E. Brus, and T. F. Heinz, Direct measurement of the lifetime of optical phonons in single-walled carbon nanotubes, Phys. Rev. Lett. **100**, 225503 (2008).

[24] H. Yan, D. Song, K. F. Mak, I. Chatzakis, J. Maultzsch, and T. F. Heinz, Time-resolved Raman spectroscopy of optical phonons in graphite: Phonon anharmonic coupling and anomalous stiffening, Phys. Rev. B **80**, 121403(R) (2009).

[25] K. Kang, D. Abdula, D. G. Cahill, and M. Shim, Lifetimes of optical phonons in graphene and graphite by time-resolved incoherent anti-Stokes Raman scattering, Phys. Rev. B **81**, 165405 (2010).

[26] S. Wu, W.-T. Liu, X. Liang, P. J. Schuck, F. Wang, Y. R. Shen, and M. Salmeron, Hot phonon dynamics in graphene, Nano Lett. **12**, 5495 (2012).

[27] R. B. Versteeg, J. Zhu, P. Padmanabhan, C. Boguschewski, R. German, M. Goedecke, P. Becker, and P. H. M. van Loosdrecht, A tunable time-resolved spontaneous Raman spectroscopy setup for probing ultrafast collective excitation and quasiparticle dynamics in quantum materials, Struct. Dyn. **5**, 044301 (2018).

[28] N. Pellatz, S. Roy, J. W. Lee, J. L. Schad, H. Kandel, N. Arndt, C. B. Eom, A. F. Kemper, and D. Reznik, Relaxation timescales and electron-phonon coupling in optically pumped $YBa_2Cu_3O_{6+x}$ revealed by time-resolved Raman scattering, Phys. Rev. B **104**, L180505 (2021).

[29] K. Katsumi, A. Alekhin, S.-M. Souliou, M. Merz, A.-A. Haghighirad, M. Le Tacon, S. Houver, M. Cazayous, A. Sacuto, and Y. Gallais, Disentangling lattice and electronic instabilities in the excitonic insulator candidate Ta_2NiSe_5 by nonequilibrium spectroscopy, Phys. Rev. Lett. **130**, 106904 (2023).

[30] T. Mertelj, J. Demsar, B. Podobnik, I. Poberaj, and D. Mihailovic, Photoexcited carrier relaxation in $YBa_2Cu_3O_{7-\delta}$ by picosecond resonant Raman spectroscopy, Phys. Rev. B **55**, 6061 (1997).

[31] D. Tuschel, Raman thermometry, Spectroscopy **31**, 8 (2016).

[32] See Supplemental Material at http://link.aps.org/supplemental/10.1103/PhysRevB.109.195141 for the details of experimental setup; background subtraction, and peak fitting model; probe fluence-dependent measurements and the procedure of extracting zero-fluence phonon temperatures; deconvolution of lattice temperatures; and the details of heating calculation, which includes Refs. [33,34].

[33] A. Gupta, A. Kumari, S. K. Verma, and B. D. Indu, The phonon and electron heat capacities of cuprate superconductors, Phys. C (Amsterdam, Neth.) **551**, 55 (2018).

[34] A. Jiříčková, F. Antončík, M. Lojka, D. Sedmidubský, and O. Jankovský, Heat capacity and thermal stability of $YBa_2Cu_3O_7$, AIP Conf. Proc. **1988**, 020018 (2018).

[35] A. F. G. Wyatt, V. M. Dmitriev, W. S. Moore, and F. W. Sheard, Microwave-enhanced critical supercurrents in constricted tin films, Phys. Rev. Lett. **16**, 1166 (1966).

[36] G. M. Éliashberg, Film superconductivity stimulated by a high-frequency field, Pis'ma Zh. Eksp. Teor. Fiz. **11**, 186 (1970) [Sov. Phys. JETP Lett. **11**, 114 (1970)].